Effect of intervalley interaction on band topology of commensurate graphene/EuO heterostructures

Shanshan Su, Yafis Barlas, Junxue Li, Jing Shi, and Roger K. Lake

Phys. Rev. B **95**, 075418 — Published 15 February 2017

DOI: 10.1103/PhysRevB.95.075418

The Effect of Intervalley Interaction on the Band Topology of Commensurate Graphene/EuO hetero-structures

Shanshan Su,[1,2,*] Yafis Barlas,[3,2,†] Junxue Li,[3,2,‡] Jing Shi,[3,2,§] and Roger K. Lake[1,2,¶]

[1] *Department of Electrical and Computer Engineering, University of California, Riverside, CA 92521, USA*
[2] *Center of Spins and Heat in Nanoscale Electronic systems, University of California, Riverside, CA 92521, USA*
[3] *Department of Physics and Astronomy, University of California, Riverside, CA 92521, USA*

(Dated: November 17, 2016)

Recent experiments demonstrating proximity induced ferromagnetism in graphene motivate this study of commensurate graphene/EuO hetero-structures. Due to the commensurability of graphene with the (111)-EuO layer, graphene's Dirac points are mapped to the $\mathbf{\Gamma}$ point of the commensurate Brillouin zone. The Eu atoms not only induce proximity exchange on the graphene layer, but they also introduce inter-valley interactions resulting in a non-linear dispersion at $\mathbf{\Gamma}$. We develop a model Hamiltonian, consistent with the lattice symmetries, that includes proximity induced exchange splitting, spin-orbit coupling, and inter-valley interactions with parameters fitted to *ab initio* calculations. The inter-valley interaction opens up a trivial gap preventing the system from crossing into a non-trivial state. The model Hamiltonian is analyzed to determine the conditions under which the hetero-structures can exhibit topologically non-trivial bands.

I. INTRODUCTION

Ever since the classification of the integer quantum Hall effect (IQHE) in terms of topological invariants[1], significant theoretical effort has gone towards realizing IQHE phenomenology at vanishing external magnetic fields. Haldane[2] proposed that in the presence of an intrinsic spin-orbit coupling, spinless electrons hopping on a two-dimensional honeycomb lattice are topologically non-trivial, and this can result in one-dimensional chiral gapless excitations along the edges of a gapped graphene system. Owing to the chiral nature of these edge modes, the gapless edge states are dissipationless and exhibit a Hall conductance $\sigma_{xy} = e^2/h$. This Hall conductance is a consequence of the Berry curvature associated with the Bloch bands in momentum space, and it is quantized only when the Fermi energy lies in the bulk band gap of the material. A number of other proposals have been made for realizing the quantum anomalous Hall (QAH) effect in mercury-based quantum wells[3], optical lattices[4], disorder induced Anderson insulators[5], magnetic topological insulators[6,7], and ferromagnetic graphene[8,9]. The robust nature of charge transport which identifies the QAH effect at vanishing magnetic fields might enable design of novel quantum devices for low-power electronics applications.

To realize the QAH state in realistic materials two conditions are necessary, (i) broken time reversal symmetry and (ii) topologically non-trivial bands. Since topological insulators (TIs) possess a large spin-orbit coupling[10], a route towards realizing the QAH effect is to introduce ferromagnetic ordering in TIs. Immediately following recent successes in synthesizing magnetic TIs (MTIs), transport measurements in MTIs verified the predicted e^2/h Hall conductance[6,11]. Another approach is to engineer the QAH state in ferromagnetic graphene in the presence of Rashba spin-orbit coupling[8,9]. Recently, graphene was successfully deposited on an atomically thin-film insulating ferrimagnet, yttrium iron garnet (YIG), and the transport measurements revealed an unquantized anomalous Hall effect due to proximity induced ferromagnetism[12]. Several other magnetic material/van der Waals (vdW) materials combinations (for example graphene/EuO, graphene/$BiFeO_3$ and $MoTe_2$/EuO[8,13–15]) have been proposed for possible spintronics[13,14] and valleytronics[15] applications. In these systems, ferromagnetic ordering is induced by a proximity effect. Additionally, proximity induced magnetism by a magnetic insulator allows for control of the electron and hole densities by gating. Previous theoretical studies have reported an exchange splitting gap of 36 meV in graphene/EuO hetero-structures[14].

In this paper, we construct a model Hamiltonian to analyze the effect of commensurability and the resulting zone-folding and inter-valley interaction on the topological properties of commensurate graphene/EuO hetero-structures. Such hetero-structures can be constructed by placing graphene on the (111) surface of EuO, and our model Hamiltonian is applicable to any commensurate graphene/EuO hetero-structure. For commensurate graphene/EuO hetero-structures the low-energy graphene bands at the $\mathbf{K}$ and $\mathbf{K}'$ are folded to the $\mathbf{\Gamma}$ point, which is due to the $3N \times 3N$ super-lattice of the commensurate graphene-EuO stacking. This zone-folding is accompanied by two distinct types of inter-valley interactions, determined by the position of the Eu atoms that can sit on either the bridge site or the hollow site of the graphene lattice (see Fig. 1). Our model Hamiltonian is constructed to account for the inter-valley interactions induced by the Eu atoms, along with the magnetic exchange interactions and Rashba spin-orbit coupling. The parameters for the model Hamiltonian such as the strength of the inter-valley interactions, ex-

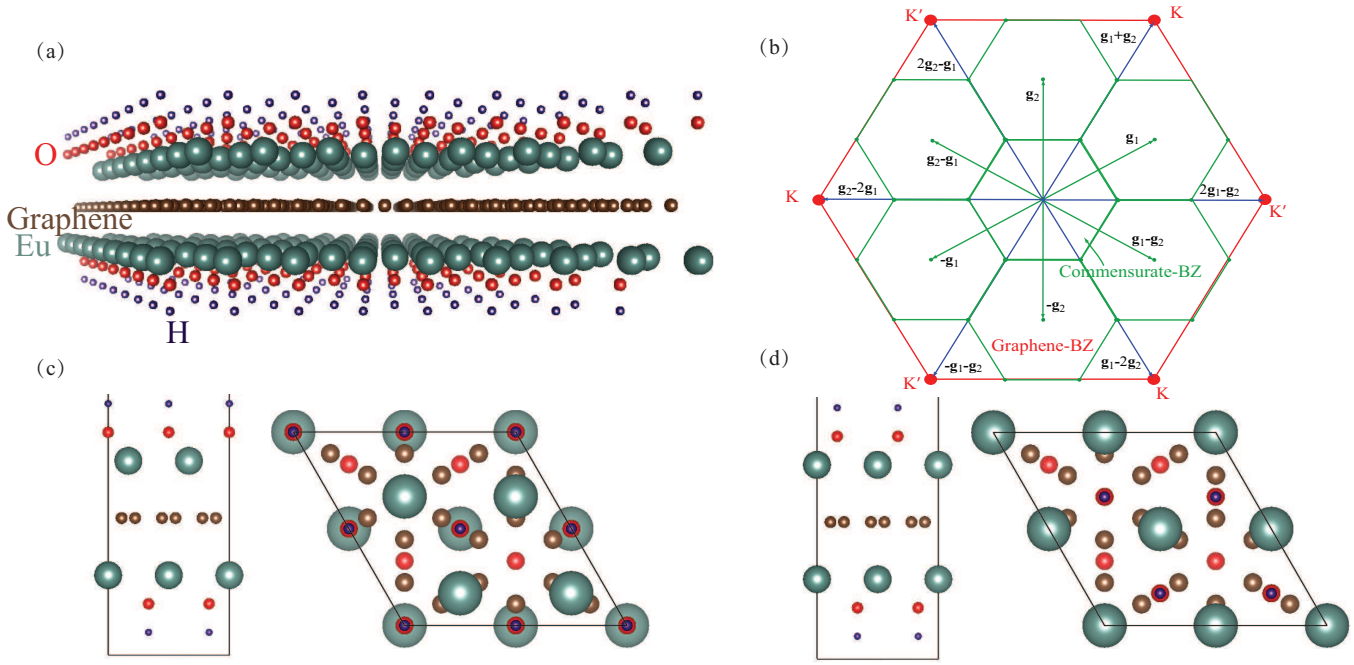

FIG. 1: (Color online) (a) Schematic view of a hetero-structure with graphene between two EuO layers. The O layers are terminated with H atoms, and the surfaces abutting the graphene are the Eu (111) planes. (b) The reciprocal lattice corresponding to the unit cells shown in (c) and (d) maps the **K** and **K′** points of the hexagonal graphene Brillouin Zone (BZ) indicated by the outer red hexagon to the **Γ** point of the commensurate BZ of the graphene/EuO unit cell indicated by the central green hexagon. The $\mathbf{g_i}$'s are the reciprocal lattice vectors of the hetero-structure unit cells in (c) and (d). Elevation and plan views of the unit cells corresponding to the two graphene/EuO geometries are shown in (c) for the Eu-misaligned structure and (d) for the Eu-aligned structure.

change splitting and spin-orbit coupling are determined by fitting to *ab initio* calculations. The low-energy band dispersion of the graphene/EuO hetero-structure depends on the strength of the inter-valley interaction terms. The position of the bridge Eu atom reduces the graphene lattice symmetry from $C_{3v} \rightarrow C_{2v}$ and results in shifting the Dirac cones from **Γ** to new points in the super-lattice Brilloun zone (BZ), whereas the Eu atoms on the hollow site open an energy gap at **Γ**. This is a topologically trivial gap that is detrimental to achieving a QAH state. We analyze the band dispersion and the topological properties of the model graphene/EuO Hamiltonian and determine conditions under which the graphene-EuO hetero-structure can acquire a non-zero Chern number.

The rest of the paper is organized as follows. In section II, we describe the two types of commensurate graphene/EuO hetero-structures and their super-lattice symmetries, and we discuss how these symmetries influence the band structure. In section III, we develop the model Hamiltonian that captures the low-energy band dispersion of the graphene/EuO hetero-structures with and without spin-orbit coupling. In section IV, calculations of the Chern numbers identify the conditions which yield topologically non-trivial bands and the QAH effect. Section V, concludes with a discussion of the possibility of proximity induced exchange and the observation of QAH effect in other graphene/ferromagnetic hetero-structures. The appendix describes *ab initio* calculations from which we extract parameters for the model Hamiltonian such as exchange splitting, spin-orbit coupling, and the values of inter-valley scattering and mass terms.

II. GRAPHENE/EUO HETERO-STRUCTURES

EuO is a ferromagnetic insulator with a Curie temperature of T_c $69K$ with a saturation magnetization of $7\mu_B$. It has a rock salt structure with the space group $Fm\bar{3}m$. Graphene is a honeycomb lattice of carbon atoms with a lattice constant 2.46 Å with the space group $P6_3mc$. In the graphene-EuO hetero-structure, the graphene lies on the Eu terminated (111) EuO surface. Each (111) layer of EuO contains 4 Eu atoms and 4 O atoms, and the Eu-layer and O-layers are stacked alternatively along the (111) direction. Each EuO layer is displaced $1.22\AA$ with respect to the adjacent layers. Twice of the lattice constant of EuO along the (111) surface is about $7.27\AA$, and it is commensurate with a 3×3 unit cell of graphene. In the combined hetero-structre the Eu atom sits either in a hollow site at the center of a graphene hexagon or at a bridge site above the center of a

C-C bond.

Figs. 1(c,d) show the two different hetero-structures studied in the paper. They differ by the alignment of the EuO-monolayer on opposite sides of the graphene layer. In both cases, graphene is placed on the (111) surface of EuO. This gives a commensurate hetero-structure with a lattice constant 2 times the lattice constant of a EuO unit cell and 3 times that of the graphene unit cell. In the aligned structure, shown in Fig. 1(d), the top EuO-monolayer is directly above the bottom EuO-monolayer, whereas in the misaligned structure shown in Fig 1(c), the top Eu-monolayer has an in-plane displacement of 1.22 Å with respect to the bottom EuO layer. In both structures the Eu atoms either sit at the center of the hexagonal graphene unit cell or at the the bridges of the C-C bonds coinciding with the inversion symmetric points of graphene's honeycomb lattice. Therefore, in-plane inversion symmetry is preserved for both cases. However, as a result of the lateral displacement of the EuO layer in the misaligned hetero-structure, inversion symmetry perpendicular to the graphene sheet is broken in contrast to the aligned hetero-structure where this symmetry is preserved. These symmetries play an important role in determining the band dispersion and the model Hamiltonian of the graphene/EuO hetero-structure.

The lattice constants of the graphene-EuO unit cell are three times those of the graphene unit cell. Hence, the reciprocal lattice constant of the commensurate BZ is $\frac{1}{3}$ that of graphene's BZ as shown Fig. 1(b). The outer hexagon (red - online) is the BZ of the graphene primitive cell, and the central hexagon (green - online) is the BZ of the hetero-structure unit cell. Fig. 1(b) shows that the **K** and **K**' points of the graphene BZ lie at equivalent $\mathbf{\Gamma}$ points in the extended zone of the hetero-structure BZ. This results in zone folding of graphene's **K** and $\mathbf{K}'$ points to $\mathbf{\Gamma}$. **This band folding leads to important changes in the band dispersion of the graphene-EuO hetero-structure, when compared to the graphene band structure (see Appendix A).** We address this next as we construct the model Hamiltonian to describe the band dispersions of the two graphene/EuO hetero-structures.

III. LOW-ENERGY EFFECTIVE HAMILTONIAN

In graphene, the gapless Dirac cones at **K** and **K'** are protected by time-reversal and inversion symmetry. Since these Dirac points are separated in the BZ, small perturbations cannot lift this valley degeneracy. Therefore, the valley index is a good quantum number. In the $3N \times 3N$ unit cell, due to zone folding of graphene's BZ, both valleys **K** and **K**' get mapped to $\mathbf{\Gamma}$. Hence, valley symmetry is no longer preserved and inter-valley interactions can gap the Dirac bands at $\mathbf{\Gamma}$ without breaking inversion or time-reversal symmetry. In the graphene/EuO hetero-structures, Eu adatoms positioned at the bridge and hollow sites contribute two distinct inter-valley interaction terms that are responsible for the non-linear dispersions obtained from the *ab initio* calculations. In this section, we construct a model Hamiltonian that captures the effect of these inter-valley interaction terms, and we analyze their effect on the band dispersion.

A. Inter-valley interactions

The following model Hamiltonian that acts on an 8 component spinor is consistent with the lattice symmetries, and it describes the salient features of the band dispersion near the $\mathbf{\Gamma}$ point in the absence of spin-orbit coupling.

$$H_0 = \hbar v_F(\hat{\sigma}_x\hat{\tau}_z p_x + \hat{\sigma}_y p_y) + \Delta_{ex}\hat{s}_z + \Delta_v\hat{\tau}_x + m\hat{\sigma}_x\hat{\tau}_x \quad (1)$$

In Eq. (1), $\hat{\tau}_i$, $\hat{\sigma}_i$ and $\hat{s}_i$ are the standard Pauli matrices acting on the valley, sublattice, and spin degree of freedom, respectively. The first term is the standard low-energy Hamiltonian describing the linear dispersion of the Dirac bands in graphene at the two valleys $\tau_z = \pm 1$ that are now folded to $\mathbf{\Gamma}$. The second term is the exchange coupling term induced by the magnetic moment of the Eu atom resulting in proximity induced exchange splitting Δ_{ex} between the spins. The last two terms of Eq. (1) capture the influence of the Eu atoms on the graphene layer. In both the hetero-structures of Fig. 1(c,d), Eu atoms can sit on a C-C bond, referred as the bridge site, and in the middle of the hexagon, referred as the hollow site. The position of the bridge Eu atom reduces the graphene lattice symmetry from $C_{3v} \to C_{2v}$ resulting in the term $\Delta_v\tau_x$ in Eq. (1). This term corresponds to a valley pseudospin Zeeman term in x-direction[16] and shifts the Dirac cones from $\mathbf{\Gamma} = (0,0)$ to $(0, \pm\Delta_v/m)$. The last term, $m\hat{\sigma}_x\hat{\tau}_x$ results from the Eu atom sitting at the hollow site of a graphene hexagon; we refer to it as an inter-valley scattering term. This term opens up a trivial gap at $\mathbf{\Gamma}$ and works against the topological transition to a non-trivial state. The combined result of these terms, along with the relative strengths of Δ_{ex}, Δ_v, and m, give a rich band dispersion and also account for the differences in the band dispersions of the two hetero-structures that we explore next.

The difference in the band dispersions of the two hetero-structures is related to the relative magnitudes of Δ_{ex}, Δ_v, and m. The energy dispersion of the model Hamiltonian H_0 is

$$E_\pm = \pm\Delta_{ex} \pm \sqrt{m^2 + v_F^2|p|^2 + \Delta_v^2 \pm 2\Delta_v\sqrt{m^2 + v_F^2 p_y^2}}, \quad (2)$$

where $|p| = \sqrt{p_x^2 + p_y^2}$. For $\Delta_{ex} = 0$ the band dispersion has two important features, if $m \geq \Delta_v$ the dispersion is elliptical and gapped at $\mathbf{\Gamma}$ ($p_x = p_y = 0$), with an energy gap $2|\Delta_v - m|$. In contrast when $\Delta_v > m$ the Dirac

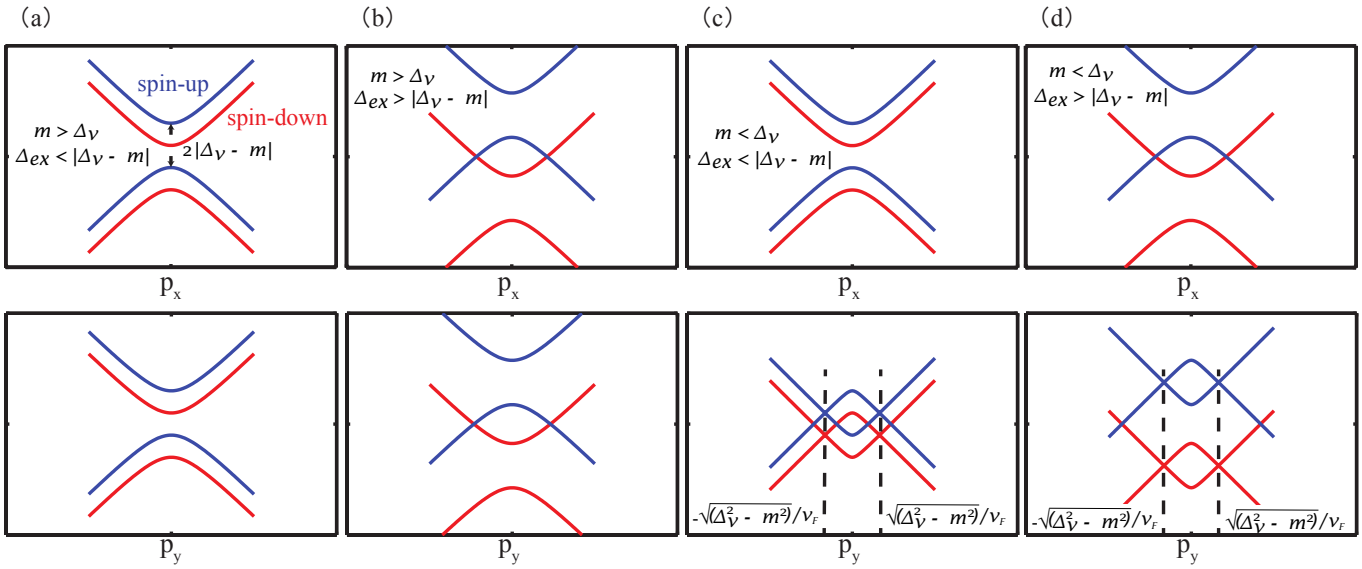

FIG. 2: (Color online) Band dispersions in the absence of spin-orbit coupling for different values of m, Δ_{ex}, and Δ_v. (a) $m > \Delta_v$ and $\Delta_{ex} < |\Delta_v - m|$, (b) $m > \Delta_v$ and $\Delta_{ex} > |\Delta_v - m|$, (c) $m < \Delta_v$ and $\Delta_{ex} < |\Delta_v - m|$, and (d) $m < \Delta_v$ and $\Delta_{ex} > |\Delta_v - m|$.

Relation between m and Δ_v	value for Δ_{ex}	band dispersion along p_x	band dispersion along p_y
$m > \Delta_v$	$\Delta_{ex} < m - \Delta_v$ in Fig. 2(a)	parabolic, spin splitting	parabolic, spin splitting
	$m - \Delta_v < \Delta_{ex}$ in Fig. 2(b)	parabolic with an overlap between spin-up and spin-down bands	parabolic with an overlap between spin-up and spin-down bands
$m < \Delta_v$	$\Delta_{ex} < \|m - \Delta_v\|$ in Fig. 2(c)	parabolic with spin splitting	two Dirac cones with spin splitting
	$\Delta_{ex} > \|m - \Delta_v\|$ in Fig. 2(d)	parabolic with an overlap between spin-up and spin-down bands	a larger overlap between the spin-up and spin-down double Dirac cones

TABLE I: Description of band dispersions in the absence of spin-orbit coupling for different parameters of Eq. (1). Plots of the dispersions corresponding to different relative strengths of the model parameters are shown in Fig. 2

points shift from $\mathbf{\Gamma}$ to $(0, \pm\sqrt{\Delta_v^2 - m^2}/v_F)$ and graphene retains its semi-metallic structure with two Dirac cones at $(0, \pm\sqrt{\Delta_v^2 - m^2}/v_F)$. For $\Delta_{ex} \neq 0$ and $m \geq \Delta_v$, there are three possibilities determined by the relative magnitudes of Δ_{ex} and $|\Delta_v - m|$. When (a) $\Delta_{ex} < |m - \Delta_v|$, there is a clear gap between the spin resolved states in Fig. 2(a). For (b) $\Delta_{ex} > |m - \Delta_v|$, the band dispersion exhibits an overlap between spin-up and spin-down bands shown in Fig. 2(b). Finally, at the transition point between scenarios (a) and (b) when $\Delta_{ex} = |m - \Delta_v|$, the elliptical bands touch. This indicates that when $m \geq \Delta_v$ there a is critical value of $\Delta_{ex} > |m - \Delta_v|$ at which the spin resolved states intersect. On the other hand, if $\Delta_{ex} \neq 0$ and $\Delta_v > m$, the shifted Dirac points which now appear at $(0, \pm\sqrt{\Delta_v^2 - m^2}/v_F)$ exhibit crossing of spin-resolved bands indicating that spin-resolved bands cross for any value of $\Delta_{ex} \neq 0$. The gap at $\mathbf{\Gamma}$ also depends on the relation between Δ_{ex} and $|\Delta_v - m|$. When $\Delta_{ex} < |\Delta_v - m|$, the band structure is shown in Fig. 2(c), and the case of $\Delta_{ex} > |\Delta_v - m|$ is shown in Fig. 2(d). Now that we have established the conditions for the intersection of spin resolved bands, we explore the results of spin-orbit coupling on the graphene/EuO heterostructures.

B. Spin-Orbit Coupling

Spin-orbit coupling introduces two additional terms consistent with the lattice symmetries,

$$H_{\rm SOC} = \frac{\lambda_R}{2}(\hat{\sigma}_x\hat{s}_y\hat{\tau}_z - \hat{\sigma}_y\hat{s}_x) + \lambda_I\hat{\sigma}_z\hat{\tau}_z. \qquad (3)$$

The first term is the Rashba spin-orbit coupling which breaks inversion symmetry in the plane perpendicular to the graphene sheet. Hence, $\lambda_R = 0$ in the aligned structure. The second term is the intrinsic spin-orbit term that breaks time reversal symmetry. Therefore $\lambda_I \neq 0$ for both structures. Since in-plane inversion symmetry is preserved in both structures, we neglect the Dresselhaus spin-orbit coupling. Our calculations indicate that the strength of the spin-orbit coupling represented by λ_R and λ_I is always smaller than m, Δ_V and Δ_{ex}, so we restrict our discussions to this case. For $\lambda_R, \lambda_I < m, \Delta_V, \Delta_{ex}$, the spin-orbit coupling introduces gaps between spin-resolved bands whenever they intersect (for example see Fig. 2 (b),(c) and (d)). With the addition of spin-orbit coupling the band dispersion becomes gapped, and the bands are a linear combination of spin-up and spin-down states.

By fitting the band dispersion with spin-orbit coupling obtained from the *ab initio* calculations shown in Fig. 7, we determine the best fit parameters for our model Hamiltonian. This gives $\hbar v_F = 3.5$ eV· Å, $\Delta_{ex} = 80$ meV, $m = 48$ meV, $\Delta_v = 17$ meV, $\lambda_R = 5$ meV, and $\lambda_I = 1$ meV. The band dispersion along the path $\mathbf{\Gamma} - \mathbf{K}$ calculated from the model Hamiltonian $H = H_0 + H_{\rm SOC}$ is shown in Fig. 3. The model Hamiltonian captures all four anti-crossing gaps at about the same position in momentum space. Next, we study the topological properties of these bands obtained from H and calculate the Hall conductance for a range of band parameters.

IV. QUANTIZED ANOMALOUS HALL EFFECT IN GRAPHENE/EUO HETERO-STRUCTURES

In Ref. 8, Qiao *et. al.* found that ferromagnetic graphene in the presence of Rashba spin-orbit coupling shows the QAH effect with $\sigma_{xy} = 2e^2/h$. First principle calculations also demonstrated that this QAH phase can be engineered by doping with $3d$ or $5d$ transition-metal atoms or the proximity of a layered antiferromagentic insulator. In all cases studies thus far, the low energy bands are at the $\mathbf{K}$ and $\mathbf{K}'$ points of the hexagonal BZ, and the Hall conductance in the gap is quantized $\sigma_{xy} = 2e^2/h$ as long as $\lambda_R \neq 0$ and $\Delta_{ex} \neq 0$. In the graphene/EuO hetero-structure, as shown in sections II and III, the low-energy bands are no longer at $\mathbf{K}$ and $\mathbf{K}'$ but at $\mathbf{\Gamma}$, and inter-valley interactions significantly modify the band dispersion and hence the topological properties of the bands. Therefore, we now analyze the effect of inter-valley interactions on the topological properties of graphene/EuO structures in the presence of in-plane inversion symmetry.

The Hall conductance is calculated from the integral of the Berry curvature over the BZ of the occupied bands and can be expressed as

$$\sigma_{xy} = \frac{e^2}{\hbar} \sum_{\alpha} \int_{BZ} \frac{d^2p}{(2\pi)^2} \Theta(E_F - \epsilon_\alpha(\mathbf{p})) \Omega_\alpha(\mathbf{p}), \qquad (4)$$

where α corresponds to the band index, E_F denotes the Fermi energy, $\epsilon_\alpha(\mathbf{p})$ is the energy eigenstate, and $\Omega_\alpha(\mathbf{p})$

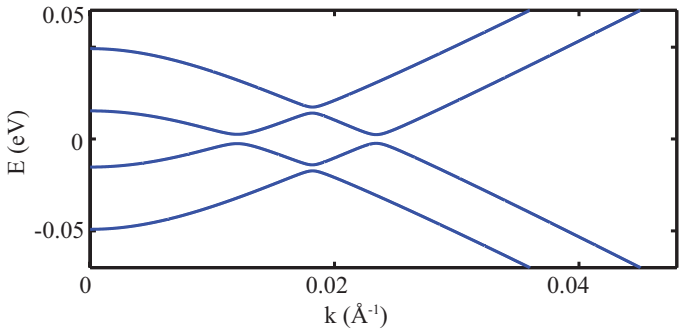

FIG. 3: Band dispersion with spin-orbit coupling of Eu-misaligned structure calculated from model Hamiltonian H along the path $\mathbf{\Gamma}$ to $\mathbf{K}$ using parameters obtained from *ab initio* calculations. $\hbar v_F = 3.5$ eV· Å, $\Delta_{ex} = 80$ meV, $m = 48$ meV, $\Delta_v = 17$ meV, $\lambda_R = 5$ meV, and $\lambda_I = 1$ meV.

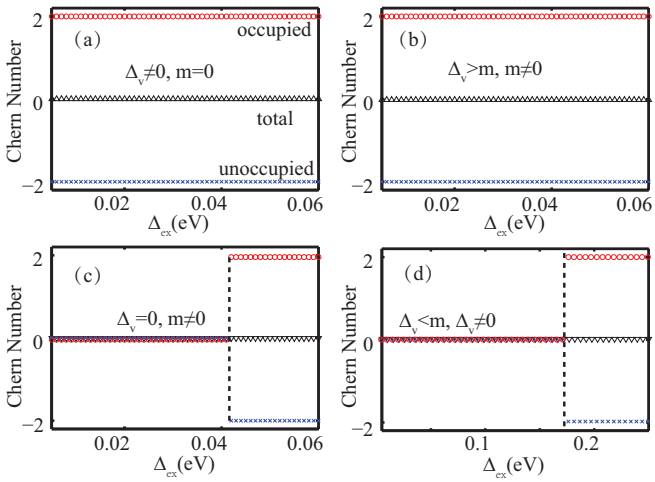

FIG. 4: (Color online) The Chern number calculated as a function of Δ_{ex} for 4 different cases of Δ_v and m. The red open circles show the Chern number of the occupied bands, the blue 'x' symbols show the Chern number of the unoccupied bands, and the black triangles show the Chern number of the summation of all bands. The Chern number of the occupied bands is 2 for all values satisfying (a) $\Delta_v \neq 0$, $m = 0$ and (b) $\Delta_v > m$, $m \neq 0$. For condition (c), $\Delta_v = 0$, $m \neq 0$, the Chern number of the occupied bands becomes 2 for $\Delta_{ex} \geq m$. For this example, m is chosen to be 0.04 eV. (d) For $\Delta_v \neq 0$ and $m > \Delta_v$, (in this example $\Delta_v = 0.01$ eV and $m = 0.04$ eV) the topological transition is pushed to a higher value of $\Delta_{ex} = 0.165$ eV.

is the Berry curvature of the α^{th} band. The Berry curvature in terms of the band eigenstates can be expressed as

$$\Omega_\alpha(\mathbf{p}) = \mathrm{Im}\sum_{\beta\neq\alpha}\left[\epsilon_{ij}\frac{\langle u_\alpha|\partial H(\mathbf{p})/\partial p_i|u_\beta\rangle\langle u_\beta|\partial H(\mathbf{p})/\partial p_j|u_\alpha\rangle}{(\epsilon_\beta(\mathbf{p})-\epsilon_\alpha(\mathbf{p}))^2}\right], \tag{5}$$

where the Einstein summation convention is used for the Roman indices i and j, ϵ_{ij} is the anti-symmetric tensor, and $u_\alpha(\mathbf{p})$ is the α^{th} band eigenstate. It is instructive to note that in-plane inversion symmetry dictates $\Omega_\alpha(\mathbf{p}) = \Omega_\alpha(-\mathbf{p})$ and time reversal symmetry imposes $\Omega_\alpha(\mathbf{p}) = -\Omega_\alpha(-\mathbf{p})$. For graphene/EuO heterostructures time reversal symmetry is broken due to exchange splitting caused by the ferromagnetic substrate, however in-plane inversion symmetry is preserved. We take advantage of the in-plane inversion symmetry by calculating the Berry curvature in the upper half-plane $p_y > 0$ and multiplying by a factor of 2 to account for the lower half-plane $p_y < 0$. The Berry curvature is calculated numerically. Our calculations satisfy that the sum of the Berry curvatures over all the bands is zero at every $\mathbf{p}$ point in the BZ, as expected from Eq. (5).

The model Hamiltonian H only captures the low-energy bands near $\mathbf{\Gamma}$ and may not be valid over the full BZ of the graphene/EuO hetero-structure. The Berry curvature calculated using (5) falls rapidly away from the $\mathbf{\Gamma}$ point. This allows us to restrict our calculations of the Hall conductance to a neighborhood of $\mathbf{\Gamma}$. It is well known that when the Fermi energy lies in the gap σ_{xy} is quantized and the Hall conductance at zero temperature can be expressed as

$$\sigma_{xy} = \frac{e^2}{h}\sum_\alpha{}' C_\alpha, \tag{6}$$

where the prime indicates summation over the occupied bands, and C_α is the Chern number of the α^{th} band that we calculate for different parameters of our model Hamiltonian H. We next discuss the Chern numbers at $E_F = 0$ for the occupied and unoccupied bands.

The calculations for the Chern numbers were performed for 4 different cases with fixed values for λ_R, m, and Δ_v (with $\lambda_R < m,\ \Delta_v$) as a function of Δ_{ex}. **For this case, λ_I is not considered.** The four different cases are depicted in Fig. 4(a)-(d). Figs. 4(a) and (b) show the results when $\Delta_v > m$. In this case the Chern number is quantized and gives a Hall conductance $\sigma_{xy} = 2e^2/h$ for any value of $\lambda_R \neq 0$. However, when $\Delta_v < m$ and $m \neq 0$, there is a topological transition as a function of Δ_{ex} and the Chern number changes from 0 to 2 as shown in Figs. 4(c,d). For $\Delta_v = 0$, the transition occurs when $\Delta_{ex} \geq m$ as shown in Fig. 4(c). For $\Delta_v \neq 0$ and $m > \Delta_v$, the transition is pushed to a higher value of Δ_{ex} as shown in Fig. 4(d). For both (c) and (d), $m = 0.04$ eV. In (d), $\Delta_v = 0.01$ eV, and the transition occurs at $\Delta_{ex} = 0.165$ eV. Unfortunately, we have been unable to find an analytical expression for the topological transition for $\Delta_v < m$. From the calculations, we conclude that the Chern number is 2 for the case of $\Delta_v > m$ and that the system undergoes a topological transition for $\Delta_v < m$ as a function of Δ_{ex}.

The results can be summarized in terms of the phase diagram shown in Fig. 5. In this calculation, $\lambda_R = 5$ meV, $\Delta_{ex} = 80$ meV and $\lambda_I = 1$ meV are constant, and the behavior of Chern number is calculated as a function of both the magnitude of the valley pseudospin Zeeman term Δ_v and the inter-valley scattering term m. As shown in Fig. 5, when $\Delta_v > m$, the Chern number is always 2 giving a Hall conductance $\sigma_{xy} = 2e^2/h$. At small values of Δ_v, a more complicated situation occurs in the region $m > \Delta_v$ of the phase diagram, however, for sufficiently large values of Δ_v, the phase transition occurs at $m > \Delta_v$ for a fixed value of Δ_{ex}. The red triangle shows the values for the bandstructure from Fig. 3 fitted to the *ab initio* calculation shown in Fig. 7. Even with EuO placed on both sides of the graphene providing a large proximity exchange coupling of 80 meV, the trivial gapping from the inter-valley scattering term, $m = 48$ meV, prevents the bandstructure from crossing over to a topologically non-trivial state.

V. CONCLUSIONS AND OUTLOOK

Using insights from first principle calculations and lattice symmetries, we constructed a model Hamiltonian to describe commensurate graphene/EuO heterostructures. In commensurate graphene/EuO structures band folding maps the Dirac cones to the $\mathbf{\Gamma}$ point of the hexagonal super-lattice BZ of the combined heterostructures. Apart from inducing proximity exchange splitting in the graphene bands, the Eu atoms also in-

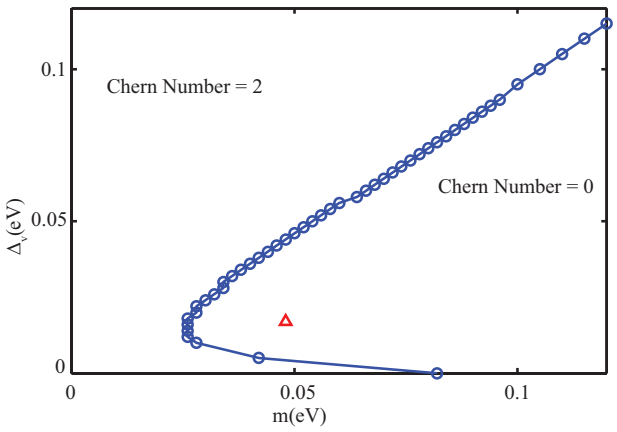

FIG. 5: Phase diagram as a fucntion of m and Δ_v for fixed values of $\lambda_R = 5$ meV, $\lambda_I = 1$ meV and $\Delta_{ex} = 80$ meV. The red triangle in the figure represents the fitted bandstructure shown in Fig. 3. The curve indicates the phase boundary between a Chern number of 2 on the left side of the curve and 0 on the right side of the curve.

troduce two distinct types of inter-valley interactions, a valley pseudospin Zeeman term and an inter-valley scattering term, whose strengths are captured by two model parameters Δ_v and m. The combined effect of exchange and inter-valley interactions results in a non-linear dispersion at the $\mathbf{\Gamma}$ point which is captured by the model Hamiltonian. The parameters of the model Hamiltonian are determined by fitting to the band dispersion obtained from the *ab initio* calculations.

Using the model Hamiltonian with Rashba spin-orbit coupling, exchange, and inter-valley interactions we calculate the band dispersion and the topological properties of the commensurate graphene/EuO hetero-structures. The inter-valley interactions can significantly influence the topological properties of the bands for non-zero Rashba ($\lambda_R \neq 0$) and exchange splitting ($\Delta_{ex} \neq 0$). For $\Delta_v > m$ with $\lambda_R,\ \Delta_{ex} \neq 0$, the commensurate graphene/EuO hetero-structure is a Chern insulator with a Hall conductance $\sigma_{xy} = 2e^2/h$, whereas for small Δ_v with $m > \Delta_v$, the phase diagram becomes more complicated and one needs a large exchange splitting or Rashba spin-orbit coupling to realize the Chern insulating phase. Our calculations indicate that even in the presence of in-plane inversion symmetry, inter-valley interactions can significantly influence the topological properties of graphene/EuO hetero-structures.

For a random incommensurate crystallographic stacking of graphene on EuO, the inter-valley coupling will be negligible since the Dirac cones will remain at $\mathbf{K}$ and $\mathbf{K}'$. However, since any incommensurate stacking will break the in-plane inversion symmetry of the graphene layer, the model Hamiltonian H would acquire an additional term $M\hat{\sigma}_z$[16]. In this case the topological properties will depend on the relative strength of M and $\Delta_{gap} < \min(\lambda_R, \Delta_{ex})$. The system will exhibit a QAH effect with a Chern number 2 only if $M < \Delta_{gap}$.

To observe the QAH effect in graphene/ferromagnet hetero-structures, it is important that the disorder induced broadening Σ of the bands be smaller than the topological band gap Δ_{gap}. The critical temperature required to observe the QAH effect is proportional to the mobility gap defined as $\Delta_{gap} - \Sigma$, which must be positive. In order to increase the topological gap Δ_{gap}, it is important to have a large Rashba spin-orbit coupling λ_R, which is small ~ 7 meV in our calculations. The Rashba spin-orbit coupling can in principle be enhanced by hydrogenation or deposition of heavy adatoms on the graphene surface[17]. Even for negative values of the mobility gap ($\Delta_{gap} - \Sigma < 0$), the graphene/ferromagnetic structures will exhibit an unquantized anomalous Hall effect. However, in this case the anomalous hall effect will be additionally influenced by disorder induced extrinsic effects[18] like side-jump and skew scattering mechanisms which are beyond the scope of this study.

VI. APPENDIX: FIRST PRINCIPLE CALCULATIONS

The band dispersions of the EuO/graphene/EuO hetero-structures are calculated using the Vienna *ab initio* simulation package (VASP)[19–21] in the projected-augmented-wave method[22]. The generalized gradient approximation (GGA) of the Perdew-Burke-Ernzerhof form[23–25] is used for the exchange correlation energy, and a Hubbard-U correction is used for the magnetic insulator, EuO. The on-site Coulomb repulsion and exchange interactions on the Eu atom $4f$ orbital are 8.3 eV and 0.77 eV, respectively, and on the O atom $2p$ orbital, they are 4.6 eV and 1.2 eV, respectively[26]. The kinetic energy cutoff is 520 eV for all calculations. During all structural relaxations, the convergence tolerance on the Hellmann-Feynman forces is less than 0.03 eV Å. An $8 \times 8 \times 8$ Monkhorst-Pack k-point mesh is used for bulk EuO. The calculated bulk lattice constant is 5.186 Å which is very close to the previously published first principle calculations[14] and consistent with the experimental results. The lattice constant a_0 of graphene is 2.46 Å. This results in a lattice mismatch of less than 1% in the $3a_0 \times 3a_0$ unit cells shown in Figs. 1(c,d).

The EuO/graphene/EuO structures consist of graphene between the (111) Eu planes of EuO. The hetero-structure with graphene on the Eu-terminated surface is more stable than graphene on the O-terminated surface[14]. The relaxation of the 2D hetero-structures uses the same level of theory, cutoffs, and tolerances as described in the previous paragraph with a Monkhorst-Pack k-point grid of $4 \times 4 \times 1$. A vacuum buffer space over 25 Å is included to prevent interaction between adjacent slabs and hydrogen atoms passivate the outer oxygen layers of the EuO films. The relaxed vertical spacing between the Eu and C layers is 2.517 Å for the

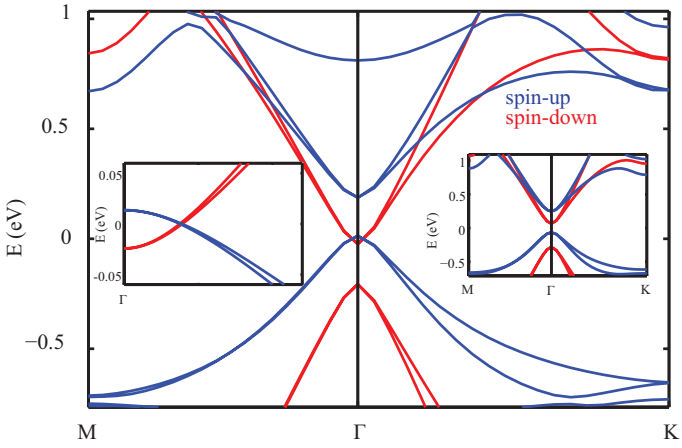

FIG. 6: (Color online) Band structure of the Eu-misaligned structure without spin-orbit coupling. Left inset: close-up of the low-energy band structure of the misaligned structure near $\mathbf{\Gamma}$. Right inset: Band structure of the Eu-aligned structure.

misaligned structure of Fig. 1(c) and 2.555 Å for the aligned structure of Fig. 1(d). These distances are close the value of 2.57 Å found previously for a single-sided hetero-structure of graphene on EuO[14].

A. Band dispersion without Spin-Orbit Coupling

Fig. 6 shows the calculated band dispersion in the absence of spin-orbit coupling for the misaligned structure of Fig. 1(c), and the right inset shows the band dispersion for the aligned structure of Fig 1(d). Both band dispersions are calculated along the path $\mathbf{M}-\mathbf{\Gamma}-\mathbf{K}$ of the commensurate BZ of the $3N\times 3N$ graphene lattice. $\mathbf{K}=(2\pi/3a, 2\sqrt{3}\pi/3a, 0)$, $\mathbf{M}=(0,\frac{2\pi}{\sqrt{3}a},0)$, and $a=7.38$ Å is the lattice constant of the hetero-structure unit cell. The most striking difference in the two band dispersions is the presence of a gap between the spin-resolved bands of the aligned hetero-structure, whereas in the misaligned hetero-structure the spin-up and spin-down bands intersect. The calculated values of gaps for both hetero-structures are tabulated in Table II. The energy band gap is denoted by E_G. The gap between the spin-up electron band and spin-up hole band is $\Delta_\uparrow$, and the gap between spin-down bands is $\Delta_\downarrow$. The spin-splitting of the electron and hole bands are δ_e and δ_h, respectively. In Table II and Fig. 6, the positive value of $E_G=127$ meV indicates a band gap between conduction and valence band, whereas the negative value of $E_G=-38$ meV indicates a spin resolved band overlap. The values of $\Delta_\uparrow$ and $\Delta_\downarrow$ in the misaligned structure are half of their values in the aligned structure. Another striking feature of the calculated band dispersion is that the low-energy bands of the combined hetero-structures appear at $\mathbf{\Gamma}$ and have curvature. In contrast, to the *ab initio* studies of a graphene/$BiFeO_3$ hetero-structure[13], the Dirac cones are no longer at the $\mathbf{K}$ and $\mathbf{K}$' points, but at $\mathbf{\Gamma}$, consistent with earlier first principle studies of graphene/EuO hetero-structures[14]. This is due to band folding.

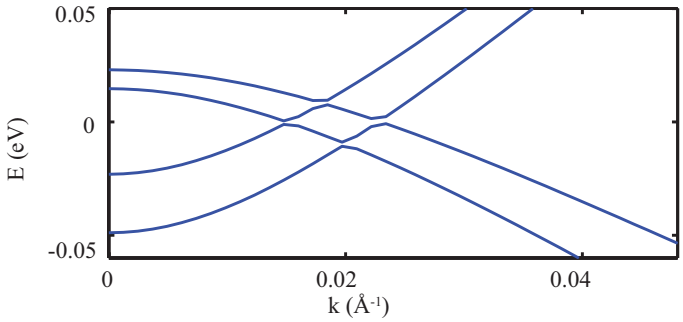

FIG. 7: (Color online) Band structure with spin-orbit coupling of Eu-misaligned structure calculated along the path $\mathbf{\Gamma}$ to $\mathbf{K}$ where $\mathbf{K}$ is 0.57 $Å^{-1}$ away from $\mathbf{\Gamma}$.

B. Band dispersion with Spin-Orbit Coupling

Our *ab initio* calculations that include spin-orbit coupling show very different behaviors of the spin resolved bands in the two hetero-structures. Since the spin-resolved bands intersect in the misaligned hetero-structure, the addition of spin-orbit coupling in this system will be more pronounced than in the aligned hetero-structure. In the aligned hetero-structure spin-orbit coupling leads to a small splitting of the spin resolved bands and the dispersion remains gapped, therefore, we focus on the effect of spin-orbit coupling in the misaligned hetero-structure.

In Fig. 7, we plot the band dispersion of the Eu-misaligned hetero-structure along path $\mathbf{\Gamma}-\mathbf{K}$. Fig. 7 shows that spin-orbit coupling breaks the degeneracy of the bands shown in the left inset of Fig. 6 and gaps the bands. The conduction bands and the valence bands split by 8 meV and 26 meV at the $\mathbf{\Gamma}$ point, respectively. There are two local minimum gaps between the conduction band and valence band in the band dispersion near $\mathbf{\Gamma}$ with values of 0.1 and 0.3 meV, respectively. The gap between the two conduction bands is 0.2 meV; while the gap between the two valance bands is 1.2 meV.

Acknowledgements: This work was supported as part of the Spins and Heat in Nanoscale Electronic Systems (SHINES) an Energy Frontier Research Center funded by the U.S. Department of Energy, Office of Science, Basic Energy Sciences under Award #DE-SC0012670. *Ab initio* calculations were also supported by FAME, one of six centers of STARnet, a Semiconductor Research Corporation program sponsored by MARCO and DARPA and used the Extreme Science and Engineering Discovery Environment (XSEDE), which is supported by the NSF grant OCI-1053575.

Structure	E_G (meV)	$\Delta_\uparrow$ (meV)	$\Delta_\downarrow$ (meV)	δ_e (meV)	δ_h (meV)
Eu aligned	127	309	344	182	217
Eu misaligned	-38	173	182	211	220

TABLE II: Energy gaps of the EuO-graphene-EuO structures at the Dirac point. E_G is the bandgap of the gapped Dirac cone. $\Delta_\uparrow$ is the spin-up gap, and $\Delta_\downarrow$ is the spin-down gap. The spin-splitting of the electron and hole bands at $\mathbf{\Gamma}$ are δ_e and δ_h, respectively.

* ssu008@ucr.edu
† yafisb@gmail.com
‡ junxue.li@ucr.edu
§ jing.shi@ucr.edu
¶ rlake@ece.ucr.edu

[1] D. J. Thouless, M. Kohmoto, M. P. Nightingale, M. den Nijs, Phys. Rev. Lett. **49**, 405 (1982).
[2] F. D. M. Haldane, Phys. Rev. Lett. **61**, 2015 (1988).
[3] C.-X. Liu, X.-L. Qi, X. Dai, Z. Fang, and S.-C. Zhang, Phys. Rev. Lett. **101**, 146802 (2008).
[4] C. Wu, Phys. Rev. Lett. **101**, 186807 (2008).
[5] C.-X. Liu, X.-L. Qi, X. Dai, Z. Fang, and S.-C. Zhang, Phys. Rev. Lett. **101**, 146802 (2008).
[6] R. Yu, W. Zhang, H.-J. Zhang, S.-C. Zhang, X. Dai, and Z. Fang, Science **329**, 61 (2010).
[7] H. Jiang, Z. Qiao, H. Liu, and Q. Niu, Phys. Rev. B **85**, 045445 (2012).
[8] Z. Qiao, S. A. Yang, W. Feng, W.-K. Tse, J. Ding, Y. Yao, J. Wang, and Q. Niu, Phys. Rev. B **82**, 161414 (2010).
[9] Z. Qiao, H. Jiang, X. Li, Y. Yao, and Q. Niu, Phys. Rev. B **85**, 115439 (2012).
[10] M. Z. Hasan and C. L. Kane, Rev. Mod. Phys. **82**, 3045 (2010).
[11] X. Kou, S.-T. Guo, Y. Fan, L. Pan, M. Lang, Y. Jiang, Q. Shao, T. Nie, K. Murata, J. Tang, Y. Wang, L. He, T.-K. Lee, W.-L. Lee, and K. L. Wang, Phys. Rev. Lett. **113**, 137201 (2014).
[12] Z. Wang, C. Tang, R. Sachs, Y. Barlas, and J. Shi, Phys. Rev. Lett. **114**, 016603 (2015).
[13] Z. Qiao, W. Ren, H. Chen, L. Bellaiche, Z. Zhang, A. H. MacDonald, and Q. Niu, Phys. Rev. Lett. **112**, 116404 (2014).
[14] H. X. Yang, A. Hallal, D. Terrade, X. Waintal, S. Roche, and M. Chshiev, Phys. Rev. Lett. **110**, 046603 (2013).
[15] J. Qi, X. Li, Q. Niu, and J. Feng, (2015), 1504.04434.
[16] Y. Ren, X. Deng, Z. Qiao, C. Li, J. Jung, C. Zeng, Z. Zhang, and Q. Niu, Phys. Rev. B **91**, 245415 (2015).
[17] J. Balakrishnan, G. Kok Wai Koon, M. Jaiswal, A. H. Castro Neto, and B. Özyilmaz, Nat Phys **9**, 284 (2013).
[18] N. Nagaosa, J. Sinova, S. Onoda, A. H. MacDonald, and N. P. Ong, Rev. Mod. Phys. **82**, 1539 (2010).
[19] G. Kresse and J. Furthmüller, Phys. Rev. B **54**, 11169 (1996).
[20] G. Kresse and J. Hafner, Phys. Rev. B **47**, 558 (1993).
[21] G. Kresse and J. Furthmüller, Computational Materials Science **6**, 15 (1996).
[22] P. E. Blöchl, Phys. Rev. B **50**, 17953 (1994).
[23] J. P. Perdew, J. A. Chevary, S. H. Vosko, K. A. Jackson, M. R. Pederson, D. J. Singh, and C. Fiolhais, Phys. Rev. B **46**, 6671 (1992).
[24] Y. Wang and J. P. Perdew, Phys. Rev. B **44**, 13298 (1991).
[25] G. Kresse and D. Joubert, Phys. Rev. B **59**, 1758 (1999).
[26] N. J. C. Ingle and I. S. Elfimov, Phys. Rev. B **77**, 121202 (2008).